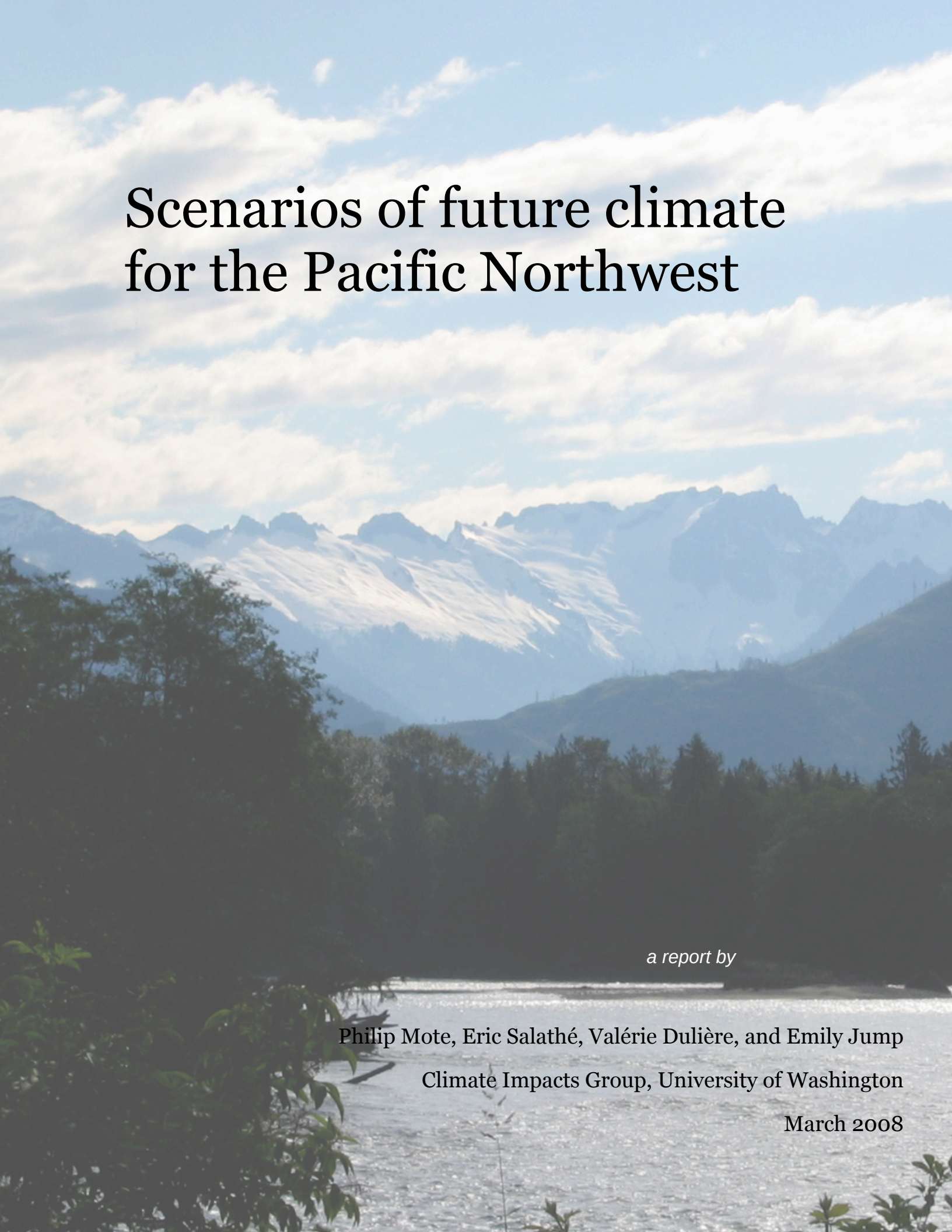

Scenarios of future climate for the Pacific Northwest

a report by

Philip Mote, Eric Salathé, Valérie Dulière, and Emily Jump

Climate Impacts Group, University of Washington

March 2008

Summary.

The average warming rate in the Pacific Northwest during the next ~50 yr is expected to be in the range 0.1-0.6°C (0.2-1.0°F) per decade, with a best estimate of 0.3°C (0.5°F) per decade. For comparison, observed warming in the second half of the 20th century was approximately 0.2°C per decade. Trends in temperature already stand out above natural variability. Projected warming is greater in summer than in other seasons.

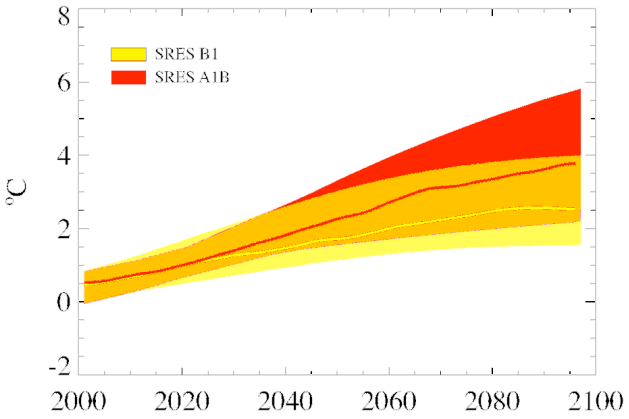

Present-day patterns of greenhouse gas emissions constrain the rate of change of temperature for the next few decades: humans are committed to some degree of additional climate change. Beyond mid-century, the projections of warming depend increasingly on emissions in the next few decades and hence on actions that would limit or increase emissions.

Projected precipitation changes are modest, and are unlikely to be distinguishable from natural variability until late in the 21st century. Most models have winter precipitation increasing and summer precipitation decreasing. Early results suggest an increase in intense precipitation but little change in coastal upwelling.

2020s*	temperature	precipitation
low	0.6°C (1.1°F)	-9%
average*	1.2°C (2.2°F)	+1%
high	1.9°C (3.4°F)	+12%
2040s*	temperature	precipitation
low	0.9°C (1.6°F)	-11%
average*	2.0°C (3.5°F)	+2%
high	2.9°C (5.2°F)	+12%
2080s*	temperature	precipitation
low	1.6°C (2.8°F)	-10%
average*	3.3°C (5.9°F)	+4%
high	5.4°C (9.7°F)	+20%

* In this document, "2020s" means the 2010-2039 average minus the 1970-1999 average, similarly for 2040s and 2080s. Model values are weighted to produce the "average".

1. Global climate models

More than 20 research centers around the world have developed and used very sophisticated models, which simulate global climate. A common set of simulations using these models was coordinated through the Intergovernmental Panel on Climate Change (IPCC), described in the IPCC 2007 report (Randall et al. 2007), and archived by the Program for Climate Model Diagnostics and Intercomparisons (PCMDI). These models typically resolve the atmosphere with between 6,000 and 15,000 grid squares horizontally, and with between 12 and 56 atmospheric layers. All models in the PCMDI archive include a fully resolved global ocean model, usually with higher resolution than the atmospheric model, and nearly all include models of sea ice dynamics and models of the land surface. By calculating energy fluxes between the sun, atmosphere, and surface, these models compute surface temperature distributions that compare well with observations. Details of the models, as well as references, can be found in Randall et al. 2007 (Table 8.1, pp 597-599).

In order to simulate 21st century climate, global climate models (GCMs) are run with different scenarios produced by the IPCC of socioeconomic change. The IPCC's six "illustrative scenarios (of which four are shown in Figure 1) lead to different scenarios of greenhouse gas and sulfate aerosol emissions and hence of climate "forcing" or energy input (watts per square meter, the y-axis in Figure 1). Sulfate aerosols promote cloud formation in certain regions and partly offset greenhouse warming. Three emissions scenarios were most frequently chosen by global modeling groups in their simulations of future climate: A2, A1B, and B1. The climate forcing of all scenarios is similar until mid-century owing primarily to the long lifetime of coal-fired electric power plants and of the major greenhouse gases. As Figure 1 clearly shows, A2 produces the highest climate forcing by the end of the century. Before mid-century, however, none of the scenarios is consistently the highest. Because more modeling groups ran A1B than A2, and since our focus for this study was on mid-century change, we chose A1B as the high emissions scenario and B1 as the low for our analysis of 21st century PNW climate. We have analyzed available A2 runs as well, as shown in Figure 8, but we emphasize A1B and B1.

We note the possibility that emissions may fall below or above the range presented here. B1 is the lowest of the IPCC illustrative scenarios, but still produces changes in climate that many scientists call "dangerous" — a threshold that a growing number of political leaders have stated their intention to avoid. At the high end, scenario A1FI (not shown) results in even higher climate forcing by 2100 than A2 or A1B. Recent global emissions of CO_2 have been exceeding even the A1FI scenario. Whether these exceedingly high emissions will continue into the future is beyond our expertise to judge.

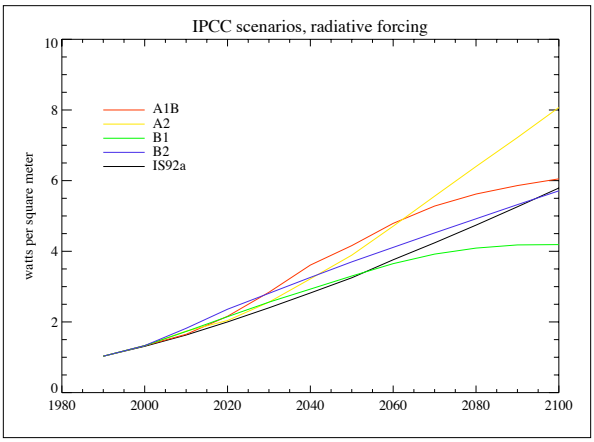

Figure 1. Globally averaged radiative forcing by greenhouse gases and sulfate aerosols, for four of the six illustrative scenarios plus the older IS92a scenario, from IPCC (2001) Appendix II.3.

From the PCMDI web site[2], all modeling centers provided simulations of 20th century climate using observed solar, volcanic, and greenhouse gas forcing. Twenty modeling centers provided simulations of 21st century climate with the A1B scenario, 19 with B1, and 17 with A2, for a total of 56 runs. In some cases several different model runs were provided for each scenario; we chose Run 1 except as noted in Appendix A. Model output was obtained from PCMDI as monthly values (and daily too for two models), and analyzed at the University of Washington by the authors of this report.

Randall et al. (2007) evaluated the models' fidelity in simulating various aspects of global climate, and also calculated each model's climate sensitivity. The modeled climate sensitivity is a measure of the model's response to doubled carbon dioxide (CO_2), and has historically been calculated in two ways: either the "equilibrium climate sensitivity" or the "transient climate response" (TCR). The equilibrium climate sensitivity is defined as the globally averaged temperature change in a simulation with a doubling of CO_2, in which the simulation is long enough for the global temperature to reach equilibrium. Because the climate system takes a long time to come into equilibrium, the calculation of the equilibrium climate sensitivity was typically performed only in models with a very simple ocean component, which was standard before the mid-1990s. By the late 1990s, most models included a sophisticated ocean, and running such a model to equilibrium would require a great deal of computer resources. The TCR was a more practical metric of models' sensitivity. The TCR is defined as the global mean temperature change at the time of CO_2 doubling in a simulation in which the CO_2 increased at 1%/year (roughly IS92a, the black curve in Figure 1). The range of values of TCR reported by Randall et al. (2007) was 1.2-2.6°C (our Table 1, their Table 8.2).

[2] URL esg.llnl.gov

nationality	model	equilibrium sensitivity	TCR
	BCCR	n.a.	n.a.
	CCSM3	2.7	1.5
	CGCM (T47)	3.4	1.9
	CGCM (T63)	3.4	n.a.
	CNRM	n.a.	1.6
	CSIRO	3.1	1.4
	ECHAM5	3.4	2.2
	ECHO-G	3.2	1.7
	FGOALS	2.3	1.2
	GFDL-CM2.0	2.9	1.6
	GFDL-CM2.1	3.4	1.5
	GISS-AOM	n.a.	n.a.
	GISS-ER	2.7	1.5
	HADCM3	3.3	2.0
	HADGEM1	4.4	1.9
	INMCM	2.1	1.6
	IPSL	4.4	2.1
	MIROC	4.0	2.1
	MIROC-hires	4.3	2.6
	PCM	2.1	1.3

Table 1. Equilibrium sensitivity and TCR (°C) as reported by Randall et al. (2007) for models used in this study.

2. Model evaluation: 20th century climate of the Northwest

In any prediction exercise the first question should be, how well can the predictive model simulate the past? In this section we examine the 20 models' simulation of 20th century climate in the Pacific Northwest.

For most of this study the Pacific Northwest is defined as the region between 124° and 111° west longitude, 41.5° to 49.5° north latitude: Washington, Oregon, Idaho, western Montana, and a small slice of adjacent states and British Columbia. Models have different resolutions, but the number of model grid points enclosed in this latitude-longitude box is between 6 and 91. We simply average the temperature and precipitation values at all the Northwest grid points to define a regionally averaged time series. The reason for such averaging is that variations in model climate on scales smaller than a few grid cells is small and not meaningful. Put another way, the models represent the variations of climate that would occur on a smooth planet with similar land-sea distributions and large smooth bumps where Earth has major mountain ranges.

Besides model resolution, another consideration in comparing global models with observations is that there are different ways to calculate "observed" regionally averaged temperature and precipitation. A common approach is to average weather station data into "climate divisions" and combine the climate divisions into a state or regional average with area weighting. The drawback of this approach is that it does not account for the contribution to a regional average of high terrain, which has very few weather stations. A better estimate interpolates (horizontally) and extrapolates (vertically) observations to a uniform, high-resolution grid (e.g., Hamlet and Lettenmaier 2005). Such an estimate, however, would be unsuitable for comparing with climate model output, which lacks the vertical relief.

A third approach is to assimilate observed data into a weather prediction model at the spatial resolution of climate models, as has been done for the NCEP/NCAR reanalysis. Because this approach processes observations is most similar to a global climate model, it is the one we define as "observations" for evaluating the model output.

We begin with a comparison of the means from models and NCEP for 1970-99, a quantity referred to as "bias." These model means will also be the reference for discussing climate changes in section 3, thereby removing most of the effects of model errors. Most models are slightly colder than NCEP — in the parlance of climate modelers, they have a "cold bias" — but the mean bias is only -0.38°C (0.68°F) and the median bias is -0.87°C (Figure 2). The models with least bias in annual average temperature are MIROC, IPSL, CCSM3, GISS-AOM, and HadGEM1. For precipitation (Figure 3), almost all models have a wet bias, and for some the bias exceeds 50%. The mean bias is 16 cm (6.3", 19%). Models with lowest bias are HadCM, GISS_er, BCCR, PCM1, and CNRM. Note that no model falls in the best five for both temperature and precipitation, whereas CSIRO, GFDL2.0, and MIROC-hi fall in the bottom five for both temperature and precipitation.

The models' simulated seasonal cycle for the PNW is shown in Figure 3. For temperature, the multi-model average is usually within 1°C of observed for each month, and has a lower root-mean-square (rms) difference from observed than any model. The annual mean multi-model mean bias of -0.38°C arises from cool biases in January-March and July-September, with negligible biases in remaining months. The range of simulated temperatures (warmest minus coldest) follows a similar pattern, being generally less than 7°C for April-June and October-December.

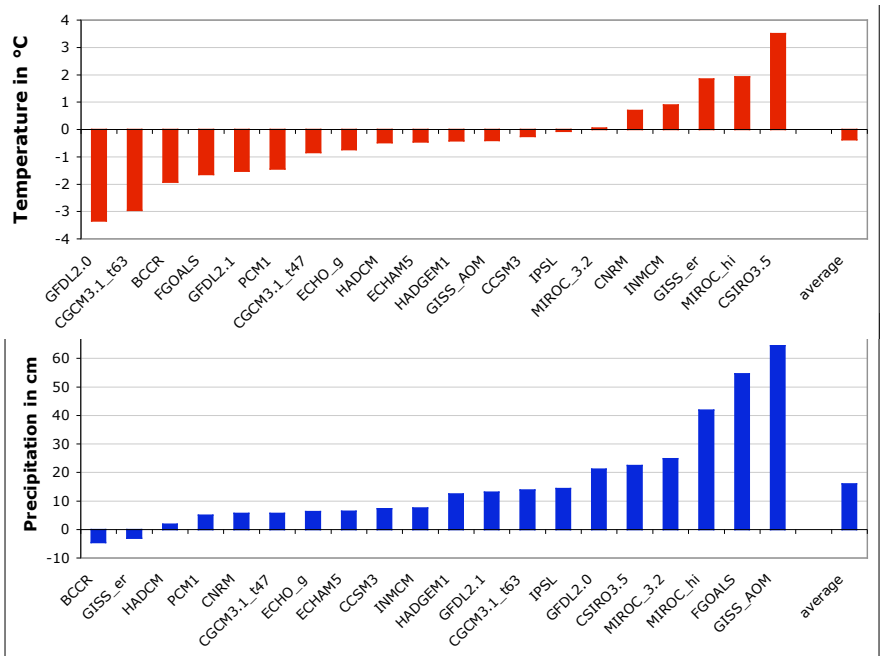

Figure 2. Biases, calculated relative to NCEP reanalysis, in each model's mean annual (top) temperature and (b) precipitation for the Pacific Northwest, for 1970-99.

For precipitation, all models reproduce the contrast between wet winters and dry summers, though a few produce summers that are only slightly drier than winters. The multi-model average is 20-30% wetter than NCEP in most months, with the largest bias (70%) in October and the smallest (<15%) in March-June. Unlike temperature, for which the multi-model average outperformed all models, nine of the models have a lower rms difference from observed than the multi-model average. HadCM has the best combined ranking followed by CNRM and ECHAM5.

Another facet of 20th century climate that can be evaluated is the trend in temperature. For the global average, many models simulate a warming rate similar to the 0.6°C warming observed in the 20th century. At the regional scale (Figure 4), the warming rate could be dominated by changes in atmospheric circulation rather than greenhouse forcing; nonetheless, eight of the models simulate a warming for the Northwest within 0.2°C of the observed warming of 0.8°C during the 20th century. We do not perform the same comparison for precipitation since there is no evidence for a 20th century response of global precipitation to greenhouse forcing. The time series of regional precipitation is characterized by high interannual variability, and the direction of linear trends depend on the start and end point, unlike temperature, for which linear trends are robustly upward.

Finally, we examine aspects of 20th century climate that pertain to the mesoscale modeling that will be reported elsewhere. Since the GCMs provide the global context for the regional modeling, the GCM fields over the domain of the mesoscale model help determine the quality of the

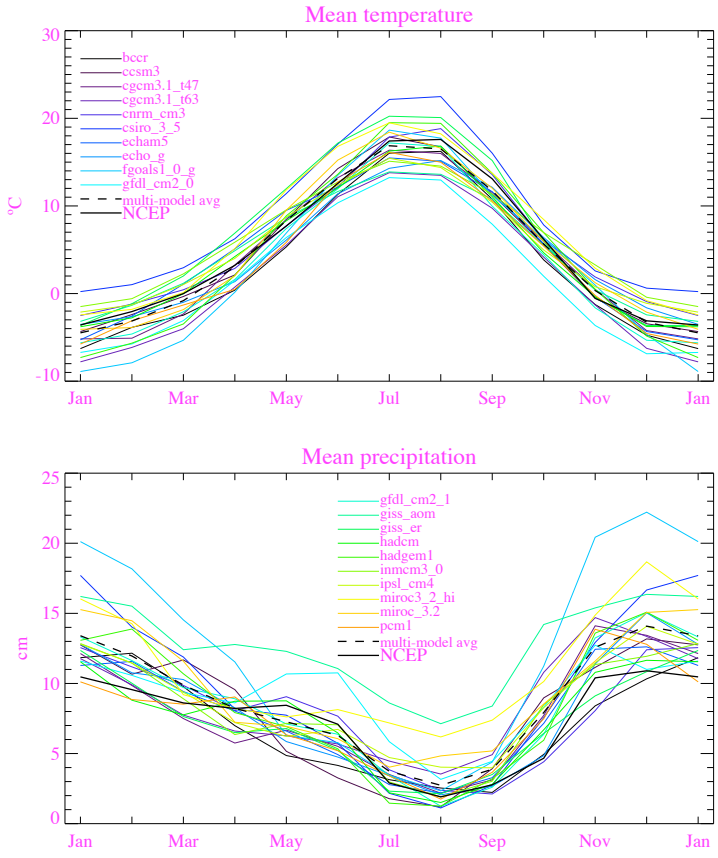

Figure 3. Mean seasonal cycle for each climate model from its 20th century simulation, compared with the NCEP/NCAR reanalysis (black). All 20 models are shown in both panels but the legend is split between the panels.

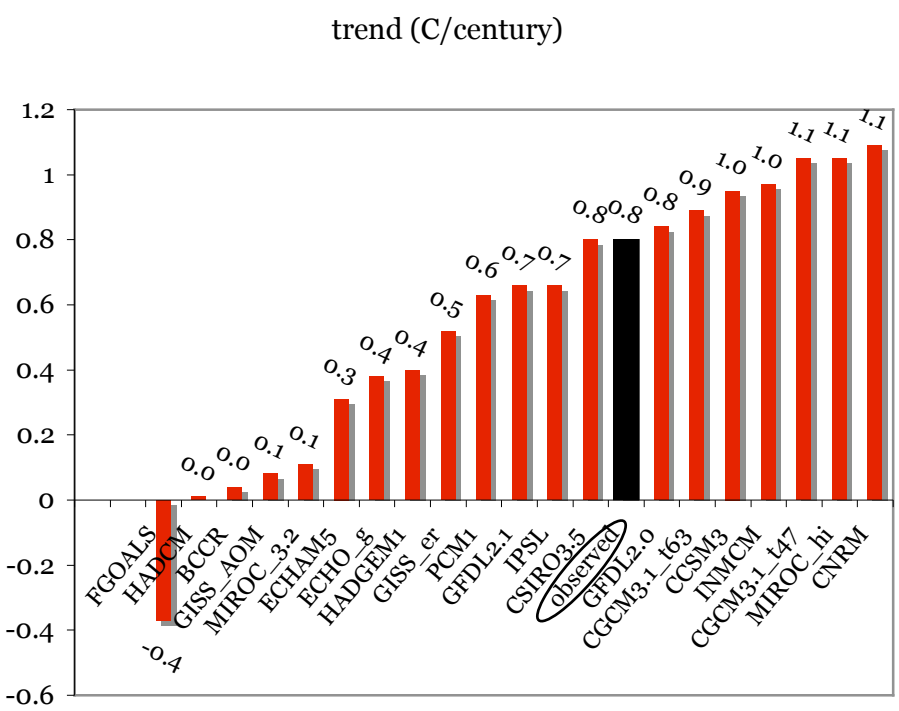

Figure 4. Trend in annual mean temperature for the PNW during the 20th century, compared with observations (black) calculated from the USHCN data.

mesoscale model simulation; in particular the moisture flux into the region provided by the GCM plays a crucial role in determining both the amount and the distribution of precipitation by the regional model.

For each model, we mapped the precipitation, sea level pressure (SLP), and temperature over roughly the domain for which we ran the mesoscale model (results of which will be reported elsewhere). Figure 5 shows the maps for one of these models, the CGCM_T47, compared with the NCEP/NCAR reanalysis. In both instances we show the annual mean for 1970-99. All models reproduce the basic features of each field: the heavy precipitation over the coastal mountains of British Columbia, the swath of high precipitation in the lower left corner, the Aleutian low and Pacific high pressure features in the middle panel, and the low temperatures over the mountainous West and the strong gradient of sea surface temperature over the western Pacific.

An efficient method of quantitatively comparing fields is the Taylor diagram (Taylor, 2000). Values are plotted in radial coordinates with the radius being the ratio of the modeled area-mean standard deviation to the observed area-averaged standard deviation, and the angle represents the spatial correlation. Figure 6 shows the Taylor diagram for all 20 models. As with global mean fields (Randall et al. 2007), of the three fields shown here temperature is best simulated by the models, with a correlation typically >0.97. Sea level pressure is next best simulated, followed by precipitation, except that for GISS-ER the SLP is worse than any model's precipitation field, owing largely to an Aleutian Low that is much too far to the west. In the Taylor diagram, the distance of a point to (1,1) represents the rms error, and we can use this distance to rank the models for each field and to average the distances to rank the models overall (Fig. 6 lower). Of all the models, CGCM-T47 (shown in Fig. 5) ranks the best.

3. Projected changes in temperature and precipitation

In addition to presenting the range of model output and the all-model average, we also present a new, *weighted* average, following the reliability ensemble averaging "REA" (Giorgi and Mearns, 2002) approach. In this approach, the REA value for each season and decade is calculated by weighting each model's output by its bias and distance from the all-model average. Multi-model averages in weather forecasting, seasonal forecasting, and climate simulations often come closer to observations than single models (see Figure 3a above), and REA should produce better results for the future than an unweighted average by giving more weight to models that perform well in simulating 20th century climate. For details on the REA calculation, see Appendix B. In this document, "2020s" denotes the 2010-2039 average, 1980s denotes the 1970-1999 average, and likewise for 2040s and 2080s.

3a. 21st century trends in the annual mean

The regionally averaged temperature and precipitation for all B1 and A1B simulations are shown in Figure 7, along with the REA value for each year. Each model's projected temperature is smoothed by regressing temperature on the logarithm of the atmospheric concentration of CO_2, an approximation of global radiative forcing (see Figure 1). The same is done for precipita-

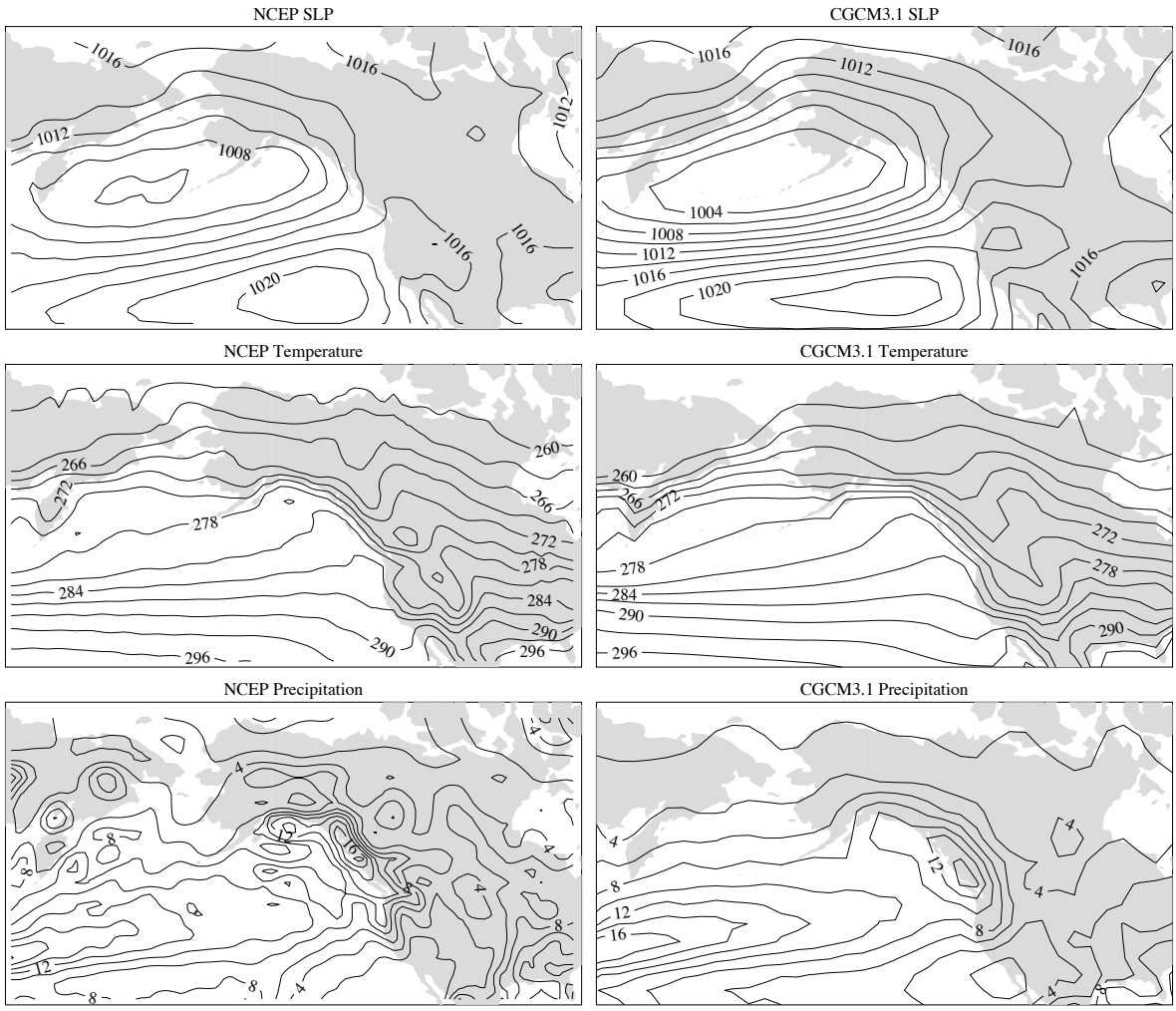

Figure 5. Annual mean patterns from (left column) CGCM-T47 and (right column) NCEP-NCAR reanalysis, for years 1950-99. Top row shows precipitation in mm/day, middle row sea level pressure in hPa, and bottom row temperature in Kelvin (273.16K=0°C=32°F).

tion. This approach highlights the region's response to the forcing on century timescales, masking model interdecadal variability which, while interesting, can confound the detection of forced change, especially for precipitation. Note how different the evolution of temperature is after about 2050 for the two scenarios, owing to the markedly different radiative forcing produced by different concentrations of greenhouse gases. By 2100 the REA value of temperature change is almost 4°C for A1B and only 2.5°C for B1. The range just for these two scenarios is 1.5 to 5.8°C; other IPCC emissions scenarios would give higher (but not lower) warming by 2100.

The observed trend in regional mean temperature is statistically significant, that is, it exceeds what would be expected from a time series with no trend and the same amount of interannual variability. Likewise, the projected future trends, even for the very lowest of the scenarios, is substantially greater than observed in the 20th century. On the other hand, for precipitation, observed and projected trends are not significant except for a few models.

Another way to view the scenarios is to plot the change in temperature on one axis and the change in precipitation on another axis (Figure 8). Figure 8 roughly shows the sensitivity of the models to forcing, with different magnitudes of forcing applied by the three SRES scenarios and in different quantities for the three decades. The ranking of models is similar for each decade and SRES scenario: HadGEM1, MIROC3_2_hi, or CCSM3 tend to be the warmest in each scenario and each decade, IPSL_CM4 or BCCR the wettest, and so on. Unlike the situation in the global mean, where the precipitation change and temperature change of models tend to be correlated, there seems to be no correspondence between temperature change and precipitation change in the Northwest. Differences among the scenarios are small in the 2020s but are substantial by the 2040s. In the coolest scenario, regional temperature rises 0.6°C (1.1°F) by the 2020s,

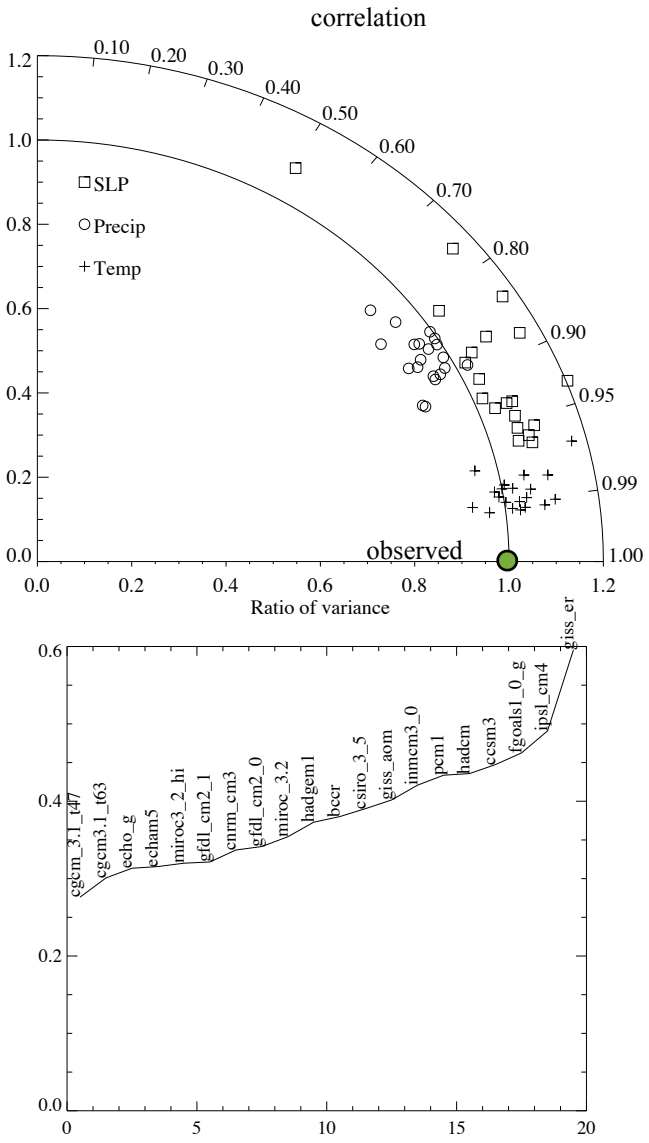

Figure 6. Evaluation of model performance over the domain shown in Figure 5. Top panel shows the correlation (angle) and ratio of variance (radius) for each model and each field. The rms difference from the observed field is just the distance on the diagram. Bottom panel ranks the models by mean distance for the three fields.

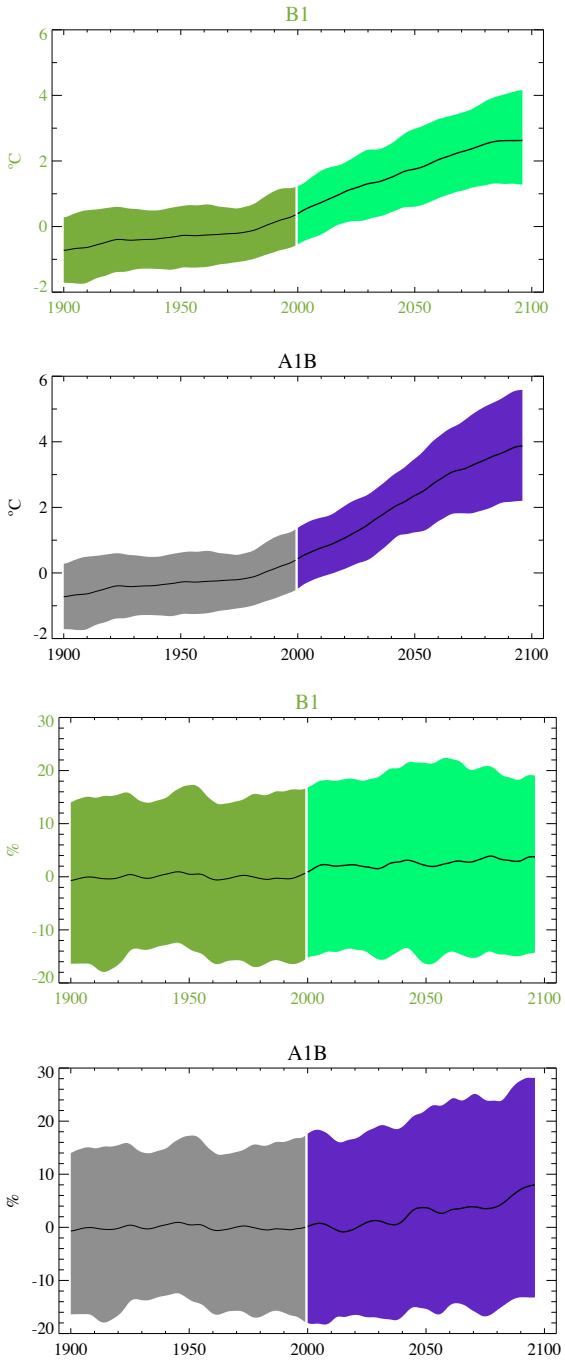

Figure 7. Smoothed traces in temperature (top two panels) and precipitation (bottom two panels) for the 20th and 21st century model simulations, relative to the 1970-99 mean. The heavy smooth curve for each scenario is the REA value, calculated for each year and then smoothed using loess. The top and bottom bounds of the shaded area are the 5th and 95th percentiles of the annual values from the ~20 simulations, smoothed in the same manner as the mean value.

0.9°C (1.5°F) by the 2040s, and 1.6°C (2.8°F) by the 2080s. In the warmest scenario, annually averaged warming is roughly a factor of three higher than the lowest scenario: 1.9°C (3.3°F) by the 2020s, 2.9°C (5.2°F) by the 2040s, and 5.4°C (9.7°F) by the 2080s.

3b. Seasonality of changes in climate

For some applications the changes of climate in a given season may be more important than the changes in annual mean. In this section we present the changes in climate by season. Figures 9 and 10 show changes in temperature and precipitation for the 2020s, 2040s, and 2080s relative to the 1980s. For both B1 and A1B, warming is expected to be largest in summer. In most seasons B1 has the lowest projected change and A1B the highest, but this is not always true in the 2020s when

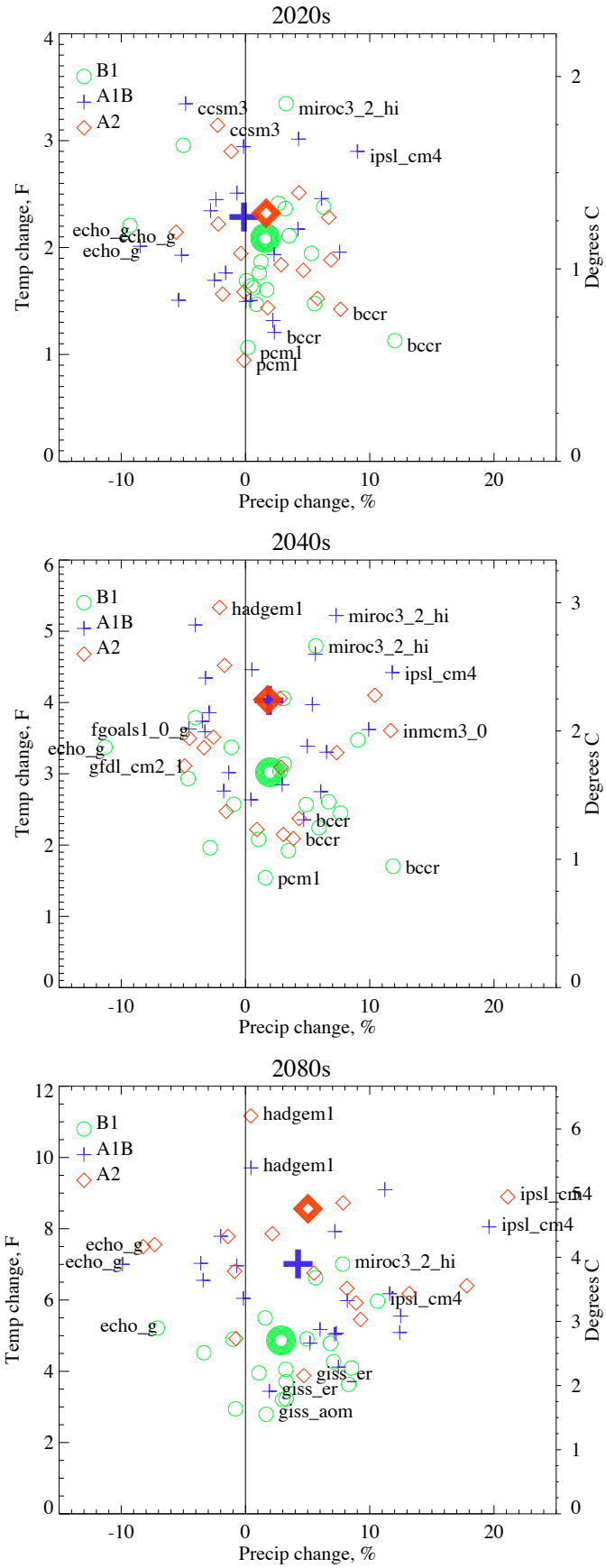

the radiative forcing of the two scenarios is very similar.

Model results for changes in precipitation are equivocal. The annual mean REA change is practically zero, though individual models produce changes of as much as -10% or +20% by the 2080s. On the seasonal scale the most consistent changes appear in the summertime, with a large majority of models (especially in the A1B scenario) projecting decreases and the REA value reaching -16% by the 2080s. Some models foresee reductions of as much as 20-40% in summer precipitation, though these large percentages only translate to 3-6 cm over the season. While small hydrologically, summer precipitation in the Northwest nonetheless has an impact on evaporative demand and hence, for example, on urban water use and forest fires.

In winter, by contrast, a majority of models project increases in precipitation. The REA value reaches +9% (about 3cm) by the 2080s for the A1B scenario, still small relative to interannual variability. And although some of the models foresee modest reductions in fall or winter precipitation, some foresee very large increases (30% or more). Changes of this magnitude would increase snow accumulation at higher elevations but would also substantially raise the risk of flooding, if the daily extremes increase along with the seasonal means.

For some applications one may want to choose a few GCM scenarios to represent a "medium" (closest to REA average), "worst case", and "best case". The worst and best case will depend very much on application, and certain seasons may matter most. For water resources impacts, the worst case scenario might be the one with the largest winter or spring warming and small or negative change in winter precipitation: for 2040s, MIROC 3.2 A1B has 2.8°C spring warming, only 3% increase in spring precipitation and no change in winter precipitation. The best case may be BCCR-B1 with a 17% increase in winter precipitation, 8% increase in spring precipitation, and warming of only 0.9°C in winter and 0.5°C in spring. Another dimension of impacts centers on how warm-dry summers are: the mean is +2.1°C and -12% for A1B, worst-case +4.4°C and -30.0% in HadCM, and best-case +0.85°C and +7% for PCM1 B1.

4. Changes in other aspects of climate

Climate models produce very detailed representations of the state of the climate system, and the IPCC data centre provides dozens if not hundreds of variables. We present here two that are relevant for coastal ecosystems and infrastructure.

Figure 8. Scatterplot of change in annually averaged temperature and precipitation for each of the 20 models and 3 SRES scenarios, for the decades indicated. Green circles indicate B1, blue crosses A1B, and red diamonds A2. Large bold symbols indicate the REA value for each scenario and decade. Model names label the four extremes for each scenario.

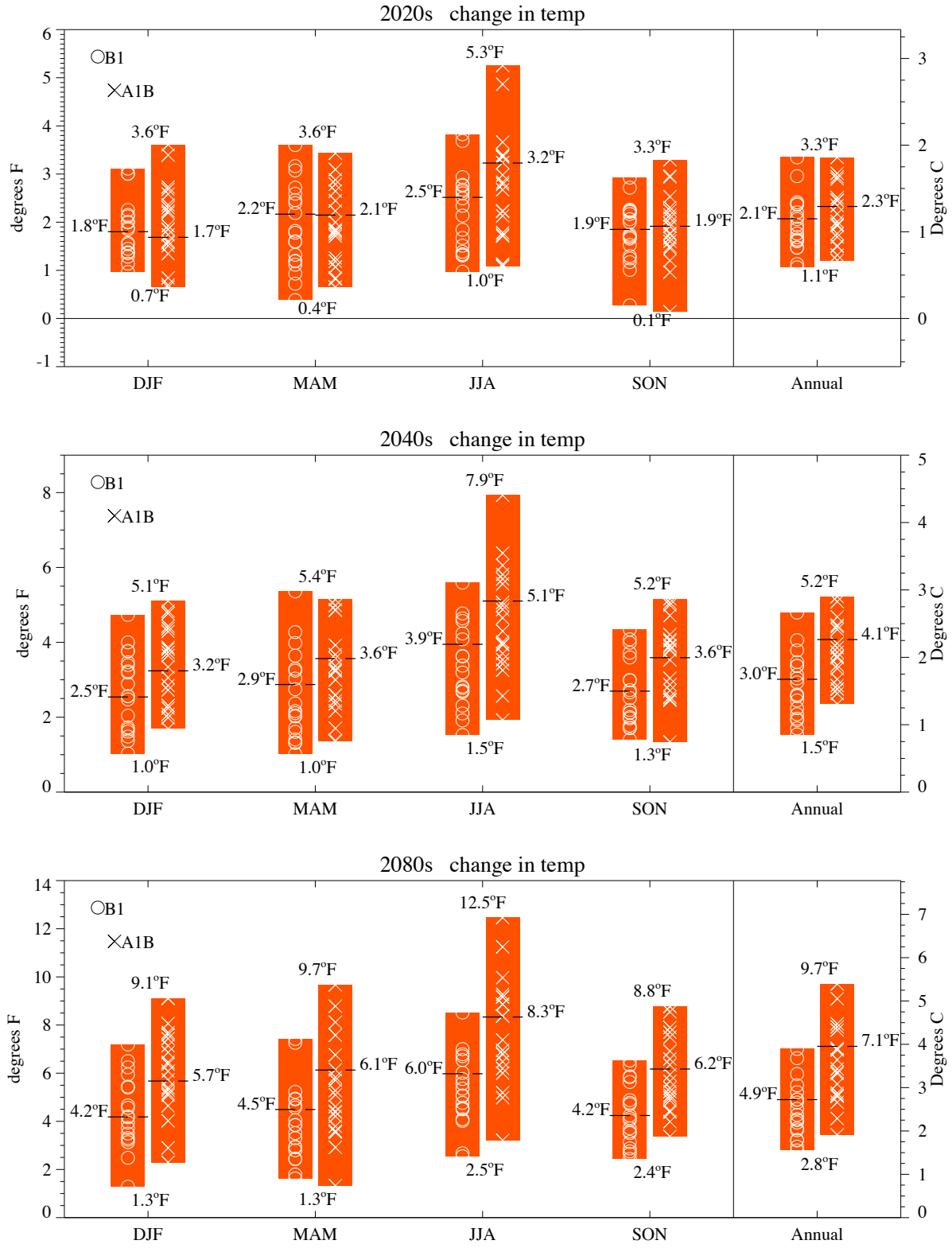

Figure 9. Range of projected changes in temperature for each season (DJF=winter, etc.) and for the annual mean, relative to the 1980s. In each pair of bars, the left one is for SRES scenario B1 and the right is A1B. The REA mean is shown as a horizontal line and the value printed. Circles and x's represent individual model values, and the highest and lowest change for each season and decade is printed.

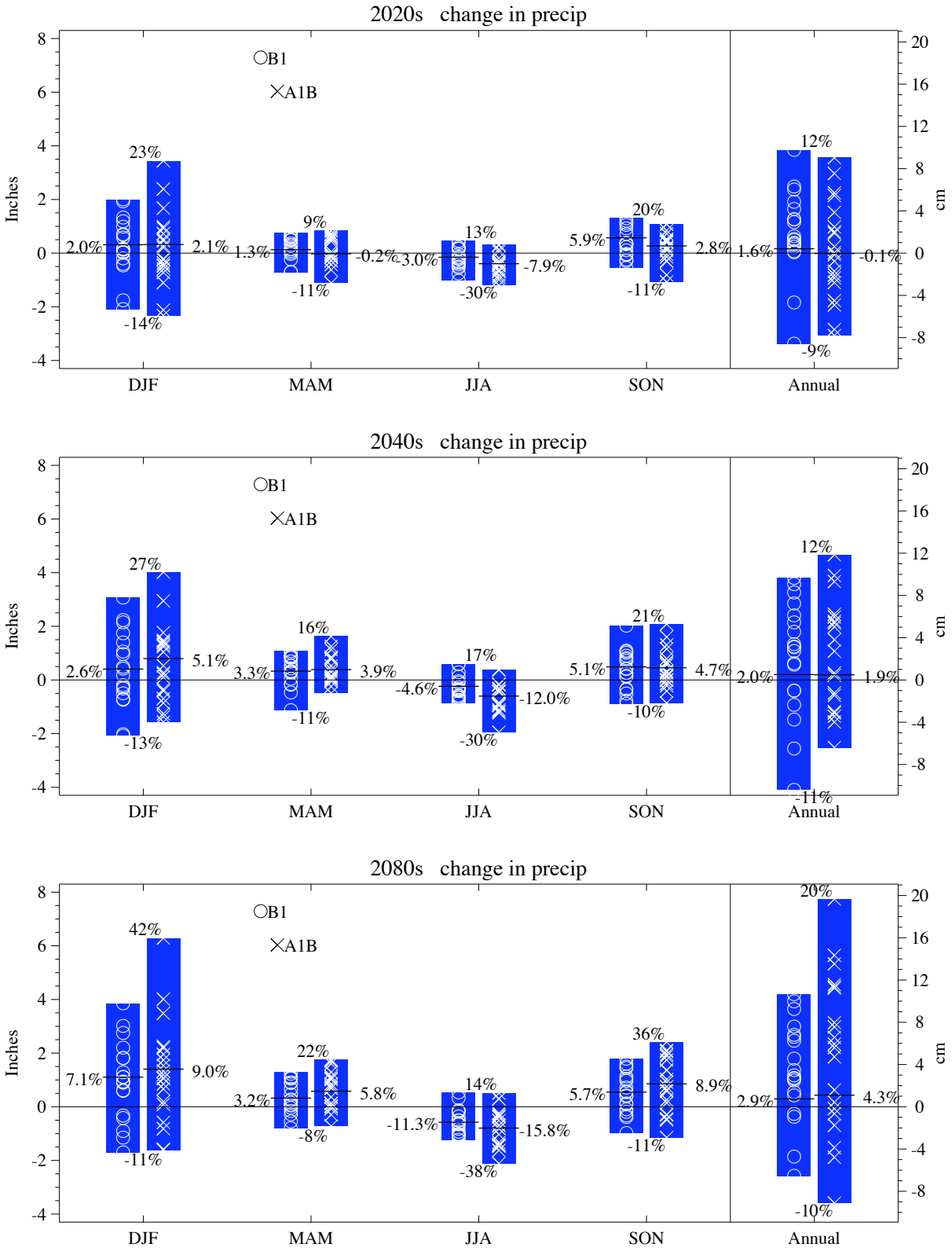

Figure 10. As in Figure 9, but for precipitation. The height of the bars indicates actual water precipitation but the percentages are calculated with respect to a reference value for *that season*, so that -11% in JJA is much less than -11% in DJF. The reference values for the extremes are that model's 20th century mean for that season (or annual mean), and for the REA average the reference is the all-model 20th century value.

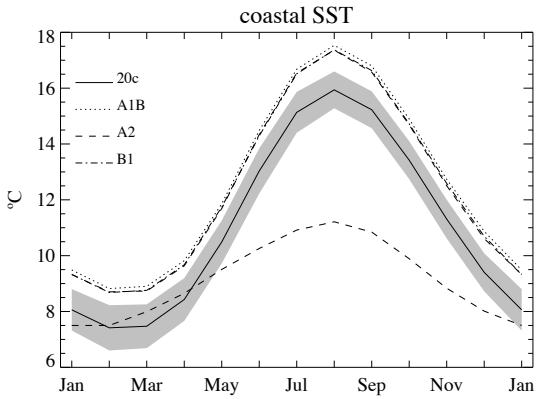

Figure 11. Simulated annual cycle of sea surface temperature (SST) averaged over 1970-99 for all available models. Grey shading represents ±1 standard deviation about the 1970-99 mean, shown as a solid black line, the three curves above the grey shaded area show the means for 2040s, and the dashed curve shows observed SST at Race Rocks near Victoria, BC, for 1970-99.

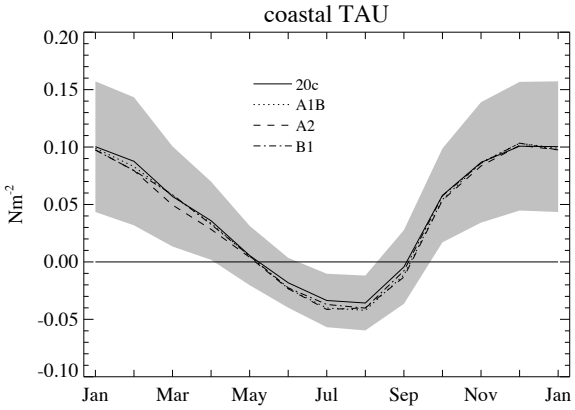

Figure 12. As in Fig. 11 but for along-shore wind stress.

4a. Coastal water properties

Coastal sea surface temperature (SST) helps determine the biological and physical conditions of the marine environment and the estuaries of the Northwest. Each of the 20 models examined here has a detailed ocean model with higher spatial resolution than the atmosphere model, and simulates SST. Figure 11 shows the mean annual cycle for the 1970-99 and 2030-59 periods for coastal grid points, along with the observed. The modeled SST is much higher than observed during the months of May-December. Modeled change is about 1.5°C, somewhat less than for the PNW land areas (2.0°C) but a significant change relative to the small interannual variability of the ocean.

Along the west coast of each continent, summertime equatorward winds pull water offshore and water must upwell from depth to replace it. This nutrient-rich water serves as the basis for very high biological productivity. Our earlier analysis of two climate models (Mote and Mantua 2002) indicated little change in coastal upwelling in any of the major regions of upwelling. For the 20 models used in this study, the mean change is also quite small (Figure 12).

4b. Changes in extreme precipitation

Daily precipitation variability is of interest because stormwater runoff and most river flooding are driven largely by extreme daily precipitation. Recent flooding events in western Washington and western Oregon in autumn 2003, 2006, and 2007 have led many to wonder whether climate change is bringing an increase in heavy precipitation events. A few modeling groups have made available their output on a daily timescale. We use daily precipitation for 1981-2000 and 2046-2065 from IPSL (the model with the largest increases in mean winter precipitation and annual precipitation) and ECHAM5 (whose winter and annual precipitation increases are close to the REA values). Figure 13 shows the extreme end of the probability distribution of precipitation for these two models. For IPSL, the probability of any given threshold being exceeded is much higher (a factor of 2 or more) in the 21st century runs than in the 20th century run. For ECHAM5 the probability of extreme precipitation increases modestly for most thresholds. These results are preliminary and further investigation of this issue will require extensive simulations with regional models.

5. Discussion of differences from previous scenarios

Previously, we analyzed ten IPCC AR4 GCM scenarios using scenarios B1 and A2 (Mote et al. 2005), and did not perform REA in constructing the "Average". Tables 2 and 3 compare the annually averaged changes derived in that effort with the changes reported here. The changes from the previous work are generally small, and the increases in the extremes are primarily the result of using A1B instead of A2. In most instances REA is fairly close to the plain model average, except in summer and in the 2080s.

temperature	2020s		2040s	
(°C)	old	new	old	new
lowest	0.4	0.6	0.8	0.9
average	1.1	1.2*	1.6	2.0*
highest	1.8	1.9	2.6	2.9

Table 2. Comparison of low, average, and high scenarios used by Mote *et al.* [2005] and this report. *In the "average" row, the old scenarios were simply averaged together but the new scenarios are combined using REA (see Appendix).

precipitation	2020s		2040s	
%	old	new	old	new
lowest	-4	-9	-4	-11
average	2	1*	2	2*
highest	6	12	9	12

Table 3. As in Table 2 but for precipitation.

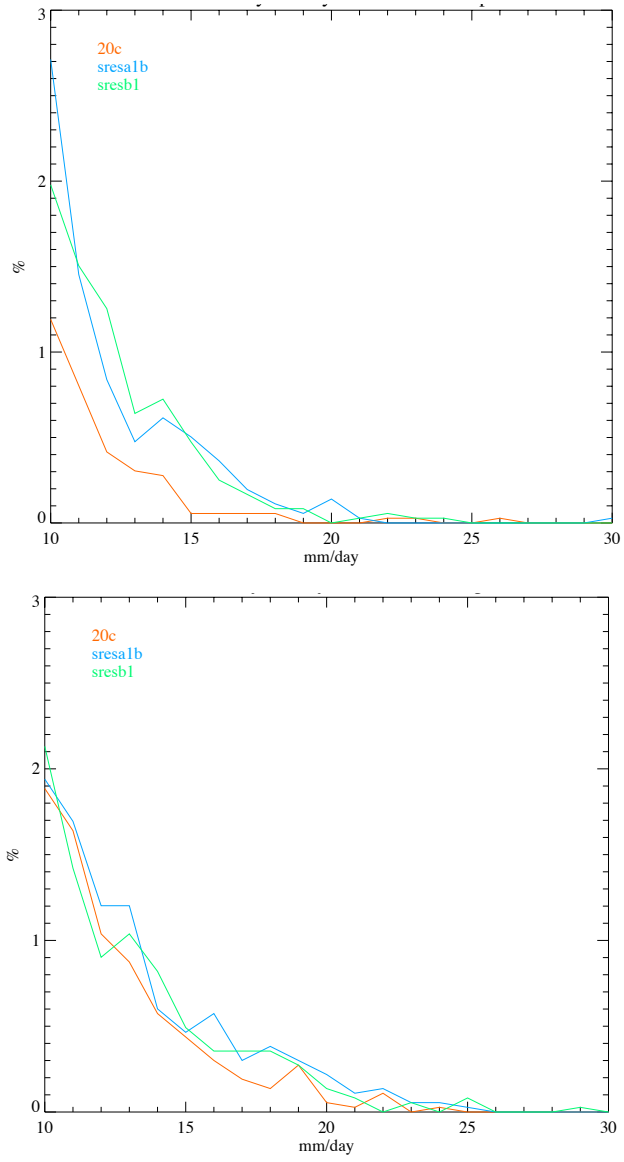

Figure 13. Probability distributions for regionally averaged daily precipitation, 1981-2000 (20c) and 2046-65, for IPSL (top) and ECHAM5 (bottom).

Appendix A. In a few instances the data available from Run 1 appeared not to be complete (e.g., missing variable or decade) so we used Run 2. The models for which this occurred were CCSM3 A2 and B1, and PCM1 B1.

Appendix B. Reliability ensemble averaging (REA) uses a bias factor and a distance factor to weight each model's output. Each factor is calculated by averaging quantities over the Pacific Northwest, for each season and for the annual mean, following these steps.

1) Compute the difference δ between the model mean and NCEP mean, for the 1970-99 period.

2) Calculate the tolerance factor ε to allow for variability of 30-year means relative to the century timescale. First, using regionally averaged data from the US Historical Climate Network, detrend (subtract the linear fit from) the 20th century time series, then calculate the standard deviation ε of the running 30-year mean. The tolerance factor is used in computing both the bias factor and the distance factor.

3) Calculate the bias factor. For models with a δ less than ε, the bias factor is 1; if δ is greater than ε, the bias factor is reduced to ε/δ.

4) Looking now at 21st century simulations, regress the quantity in question (e.g., annual mean temperature) on the log of CO2 (see Figure 1). For purposes of calculating the distance factor, take the value of the resulting fit at year 2045 minus the value at year 2000, d_i for model i. This is the only step in which we depart from the method of Giorgi and Mearns, and we do so in order that each model has a single weighting factor for each of the time periods considered (2020s, 2040s, 2080s).

5) Calculate the all-model mean value $\boldsymbol{d}$ of the individual model distances d_i. Then weight each model d_i by its distance from the mean $\boldsymbol{d}$ and recompute the all-model mean $\boldsymbol{d}$. Only one or two iterations is needed to converge.

6) Calculate the distance factor in the same manner as the bias factor: for d_i less than ε, the distance factor is 1; for d_i greater than ε, the distance factor is ε/d_i.

7) For each season, decade, scenario, and variable, compute an REA value by summing over all available models the product of the model's projected change, its bias factor, and its distance factor.

Acknowledgments. We are grateful to the Program for Climate Model Diagnosis and Intercomparison for making available the model output, and to the State of Washington for funding this work.

References

Giorgi, F., and L.O. Mearns, 2002: Calculation of average, uncertainty range, and reliability of regional climate changes from AOGCM simulations via the reliability ensemble averaging (REA) method. *J. Clim.*, 15, 1141–1158.

Hamlet, A.F., and D.P. Lettenmaier, 2005: Production of temporally consistent gridded precipitation and temperature

fields for the continental United States. *J. Hydromet.,* 6, 330-336.

Mote, P.W., and N.J. Mantua. 2002. Coastal upwelling in a warming future. *Geophysical Research Letters* 29(23), 2138 doi: 10.1029/2002GL016086.

Mote, P.W., E.P. Salathé, and C. Peacock. 2005. *Scenarios of Future Climate for the Pacific Northwest*. A report prepared for King County. Climate Impacts Group, Center for Science in the Earth System, Joint Institute for the Study of the Atmosphere and Ocean, University of Washington, Seattle.

Randall, D.A., R.A. Wood, S. Bony, R. Colman, T. Fichefet, J. Fyfe, V. Kattsov, A. Pitman, J. Shukla, J. Srinivasan, R.J. Stouffer, A. Sumi, and K.E. Taylor, 2007: Climate models and their evaluation. In: *Climate Change 2007: The Physical Science Basis. Contribution of Working Group I to the Fourth Assessment Report of the Intergovernmental Panel on Climate Change* [Solomon, S., et al., (eds.)]. Cambridge University Press, Cambridge, United Kingdom and New York, NY, USA.

Raupach, M.R., G. Marland, P. Ciais, C. Le Quéré, J.G. Canadell, G. Klepper, and C.B. Field, 2007: Global and regional drivers of accelerating CO_2 emissions. *Proc. Natl Acad. Sci.,* doi 10.1073/pnas.0700609104.

Taylor, K.E., 2000. *Summarizing multiple aspects of model performance in a single diagram*. Report No. 55 of the Program for Climate Model Diagnosis and Intercomparison, Lawrence Livermore National Laboratory.

For copies of this document, see
http://www.cses.washington.edu/db/pdf/moteetal2008scenarios628.pdf
or email philip@atmos.washington.edu

Cover photo: Skagit River with North Cascades in the background. Photo by Philip Mote.